Advanced Composites and Hybrid Materials (2022) 5:1253–1267
https://doi.org/10.1007/s42114-022-00504-4

ORIGINAL RESEARCH

Flame-retardant and leakage-proof phase change composites based on MXene/polyimide aerogels toward solar thermal energy harvesting

Yan Cao[1] · Mengman Weng[1] · M. H. H. Mahmoud[3] · Ashraf Y. Elnaggar[4] · Li Zhang[1] · Islam H. El Azab[4] · Ying Chen[1] · Mina Huang[5] · Jintao Huang[1,6] · Xinxin Sheng[1,2]

Received: 21 April 2022 / Revised: 9 May 2022 / Accepted: 24 May 2022 / Published online: 17 June 2022

Abstract

To address the problems of easy leakage and high flammability of phase change materials, a series of innovative leakage-proof phase change composites (PCCs) with excellent solar thermal conversion capability and superior flame retardancy have been successfully developed. Herein, two-dimensional layered MXene nanosheets with excellent solar-thermal conversion effect were first synthesized by etching MAX phase with lithium fluoride and hydrochloric acid solutions. MXene/polyimide (PI) aerogel was then prepared by freeze-drying and thermal imidization after MXene dispersions mixed with poly (amic acid). The MXene/PI aerogels were subsequently impregnated into polyethylene glycol (PEG) by vacuum impregnation to obtain new shape-stable MXene/PI@PEG phase change composites (MPPCCs). Among them, MPPCC-4 exhibits a very high PEG loading capacity (98.1%) and high enthalpy (167.9 J/g), and a relative enthalpy efficiency of 99.8%. When compared to PEG, MPPCC-4 has outstanding flame retardant properties, including a 26.2% lower peak heat release rate and an 11.6% lower total heat release rate. In conclusion, MPPCCs show considerable potential for application in solar energy utilization systems.

Keywords MXene · Phase change materials · Solar-thermal conversion · Thermal energy storage · Flame retardancy

1 Introduction

The shortage of fossil fuels and greenhouse gases emissions [1, 2] are exacerbated as global issues, which can be resolved through searching for new renewable energy sources [3] and developing energy-efficient systems. Among the various renewable energy, solar energy is a ubiquitous, easily accessible, and inexhaustible source to relieve energy crisis [4]. However, the application of solar energy is always restricted by several uncontrollable factors such as mismatching in time and space and low solar-thermal conversion. Therefore, exploring suitable materials making great use of solar energy is the key thesis in current research. Phase change materials (PCMs) with huge latent heat and stable phase change points are beneficial to improving the energy utilization by storing and releasing the solar energy without any environmental limitation [5]. Pure PCMs can be simply divided as organic and inorganic compounds. Compared to inorganic PCMs, organic PCMs are less corrosive and more stable to apply without phase separation during solid–liquid process [6]. However, pure organic PCMs also exist several drawbacks, which seriously hinder their practical application such as poor solar absorption and the leakage caused by deformability [7].

✉ Jintao Huang
jintao.huang@gdut.edu.cn

✉ Xinxin Sheng
xinxin.sheng@gdut.edu.cn; cexxsheng@gmail.com

1 Guangdong Provincial Key Laboratory of Functional Soft Condensed Matter, School of Materials and Energy, Guangdong University of Technology, Guangzhou 510006, China

2 Yunnan Provincial Key Laboratory of Energy Saving in Phosphorus Chemical Engineering and New Phosphorus Materials, The Higher Educational Key Laboratory for Phosphorus Chemical Engineering of Yunnan Province, Kunming 650500, China

3 Department of Chemistry, College of Science, Taif University, P.O. Box 11099, Taif 21944, Saudi Arabia

4 Department of Food Science and Nutrition, College of Science, Taif University, P.O. box 11099, Taif 21944, Saudi Arabia

5 College of Materials Science and Engineering, Taiyuan University of Science and Technology, Taiyuan 030024, Shanxi, China

6 Key Laboratory of Polymer Processing Engineering, Ministry of Education, South China University of Technology, Guangzhou 510640, China

To overcome these challenges as well as keep excellent energy storage performance, PCMs are always request to composite with other framework materials as PCMs composites. Among various preparation methods of PCM composites, encapsulated organic PCMs in porous materials is a common way to keep satisfactory shape stability and achieve stable thermal energy conversion [8]. These porous materials include graphite foam [9], carbon nanotube sponge [10, 11], graphene aerogel [12–15], expanded graphite [16–18], boron nitride aerogels [19–22], or other polymer composites [8, 23, 24]. PCMs are firmly fixed in the help of porous three-dimensional skeleton, preventing leakage via improving shape stability, which are facilitating for thermal energy storage. Unlike other common porous materials, MXene as a kind of emerging 2D materials may be also promised in PCMs composites utilization [25–27]. In contrast, MXene shows great strengths in enabling thermal energy storage and transport applications. Since 2011, MXene has been studied in many fields. It is reported that two enhanced absorption peaks have been detected in the visible and near-infrared regions, which are similar to metal nanoparticles [28, 29]. This result shows that light absorption of MXene would be enhance due to localized surface plasmon resonance effects. What is more, with excellent solar energy conversion performance, high thermal conductivity [30] and wide absorption spectral range [31], MXene is a suitable candidate for enhanced capability of solar thermal conversion [32–34]. Therefore, adding MXene in PCM-based energy storage systems will improve the utilization of solar energy.

In addition, the high flammability of organic solid–liquid PCMs (such as polyethylene glycol) is another factor severely limiting applications. Hence, it is necessary to strengthen the flame retardant performance of phase change composites (PCCs). It is understood that not only MXene have strong light absorption capacity, but it also has excellent charring capacity and physical barrier effect [35–38], which may help to improve the flame-retardant efficiency of PCCs. On the other hand, polyimide (PI) aerogels show a special three-dimensional structure, low density, and excellent flame resistance [39, 40], which is expected to be a framework material, reducing leakage and improving flame resistance of PCCs.

In this work, MXene nanosheets were obtained by etching MAX powder with lithium fluoride (LiF)-hydrochloric acid (HCl) solution. The MXene dispersion was then mixed with poly (amic acid) (PAA), followed by freeze-drying and thermal imidization to prepare MXene/PI aerogels (MPs). Finally, the MPs were vacuum-impregnated into polyethylene glycol (PEG) to obtain shape-stable MXene/PI@PEG phase change composites (MPPCCs). The solar-thermal conversion properties, thermal storage properties, thermal stability, and flame retardancy of the MPPCCs were systematically investigated. As expected, the MPPCCs have excellent shape stability and high PEG encapsulation ability (98.1%) with a relative enthalpy efficiency of 99.8%, showing strong solar-thermal conversion capability and excellent flame retardancy. Noteworthy, the peak heat release rate (pHRR) and total heat release rate (THR) of MPPCC-4 were 26.2% and 11.6% lower than pure PEG, respectively. As a result, the obtained MPPCCs have great potential in safe flame retardancy and efficient solar energy storage applications.

2 Experimental section

The manufacturing process of MPPCCs is shown in Fig. 1. First, the MAX powder was etched with LiF-HCl solution to obtain MXene nanosheets. PAA was prepared and then uniformly mixed with the MXene dispersion in a certain proportion at room temperature. After that, MPs were obtained by freeze-drying and thermal imidization. Finally, the MPPCCs were obtained by adsorbing PEG through vacuum impregnation. More detailed information on the experimental procedure and characterization can be found in the supporting information.

3 Results and discussion

3.1 Analysis of MXene

Figure 2a, b shows the morphologies of MAX (Ti_3AlC_2) powder and multilayered MXene (Ti_3C_2) powder. The Al atomic layers from the densely layered MAX phase are etched by LiF-HCl solution, and after that, the interlayer spacing becomes larger, transforming into an accordion-like loose layer structure. These phenomena are consistent with our previous research [41], indicating fluffy MXene powder with an accordion-like structure is successfully prepared. The Tyndall effect can be observed in the aqueous dispersion of MXene as shown in Fig. 2c. This indicates that MXene owns superior water dispersibility with the existing hydrophilic groups. The TEM images of single-layered MXene nanosheets are exhibited in Fig. 2d. Due to the destroyed Vander Waals force, the multilayered MXene were exfoliated as the ultra-thin MXene nanosheets. Figure 2e shows the AFM image of MXene and the corresponding height profile. The width and thickness of the MXene nanosheets are around 0.40–1.00 μm and 3.23–3.43 nm, respectively, which are consistent with those reported in the literature [42, 43]. All these results confirmed that few-layer MXene nanosheets were prepared successfully.

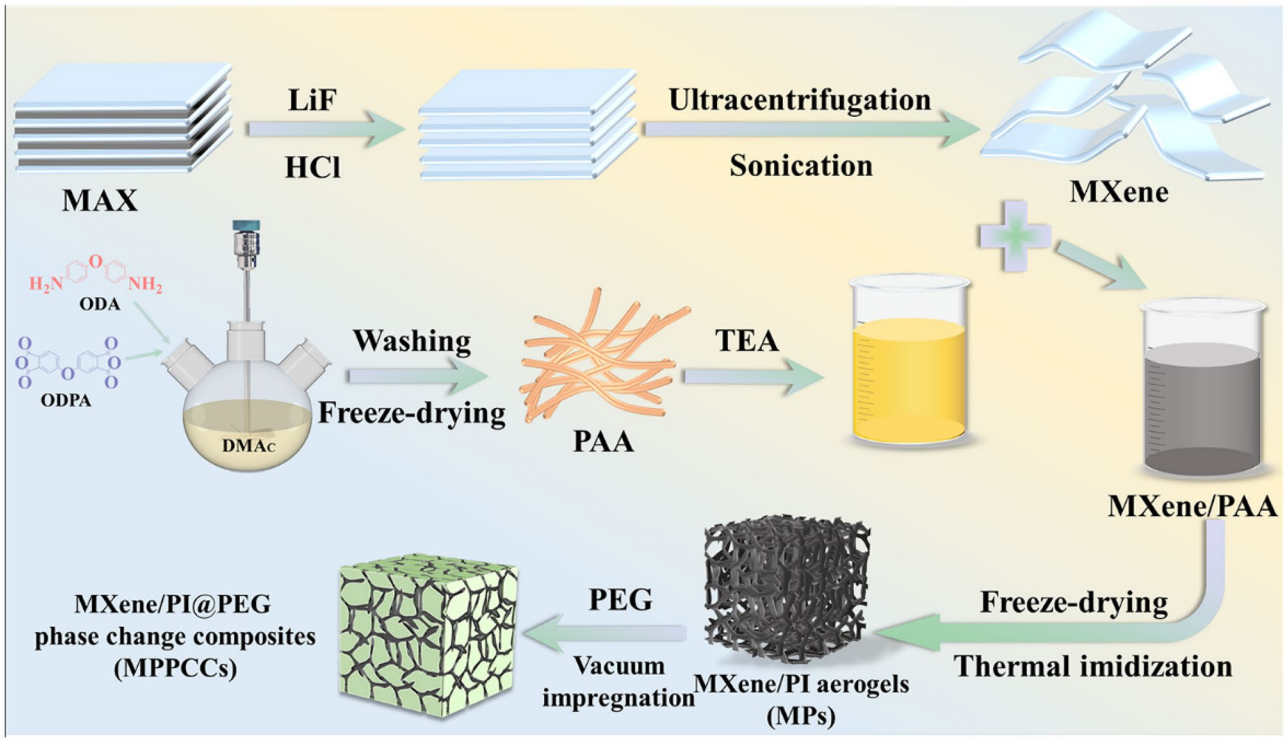

Fig. 1 MXene/PI@PEG phase change composite (MPPCC) preparation process diagram

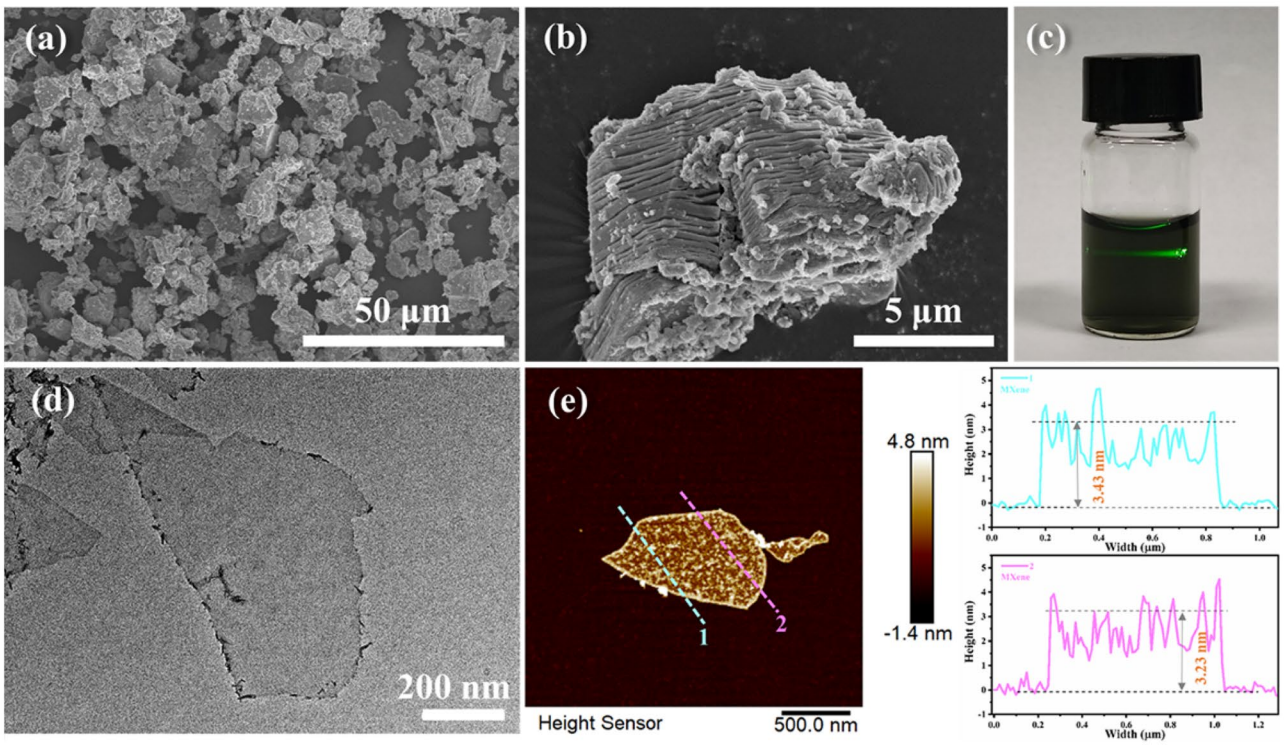

Fig. 2 SEM micrographs of **a** MAX and **b** multilayered MXene; **c** digital photo of MXene aqueous dispersion with Tyndall effect; **d** TEM images of MXene; **e** AFM images of MXene and corresponding height profiles of MXene

3.2 Morphology and structure of MXene/PI@PEG phase change composites

Figure 3a–d show SEM images of MP-5, PI aerogel and MXene aerogel. As shown in Fig. 3d, the MXene aerogel shows loose and disordered porous structure. The partially overlapping porous structures are weakly linked with the lamellar structure, so the aerogel may collapse by slight compression. At the same time, a shapeless pore structure is presented in PI aerogel (Fig. 3c). However, tight interfaces and interconnected oriented porous structures are produced after the combination of PI with MXene (Fig. 3a, b). The hydroxyl groups of MXene form strong hydrogen bonding forces with the oxygen-containing groups in the PI chains. Therefore, a stable 3D network of aerogel is formed [44]. At the same time, it can be further proved from Fig. S1 that with the increasing MXene content, the porous structure becomes more regular and denser. As shown in Fig. 3h, i, PAA solution and MXene/PAA dispersion are encased in circular boxes (radius d1), respectively. After freezing-drying, the radius of a pure PI aerogel (d2) is smaller than that of MP-4 (d4). The MP-4 is almost no change in volume after thermal imidization, while the pure PI aerogel shows severe shrinkage (d1 > d4 > d5 > d2 > d3). Therefore, these data further confirm that the MXene nanosheets are tightly wrapped

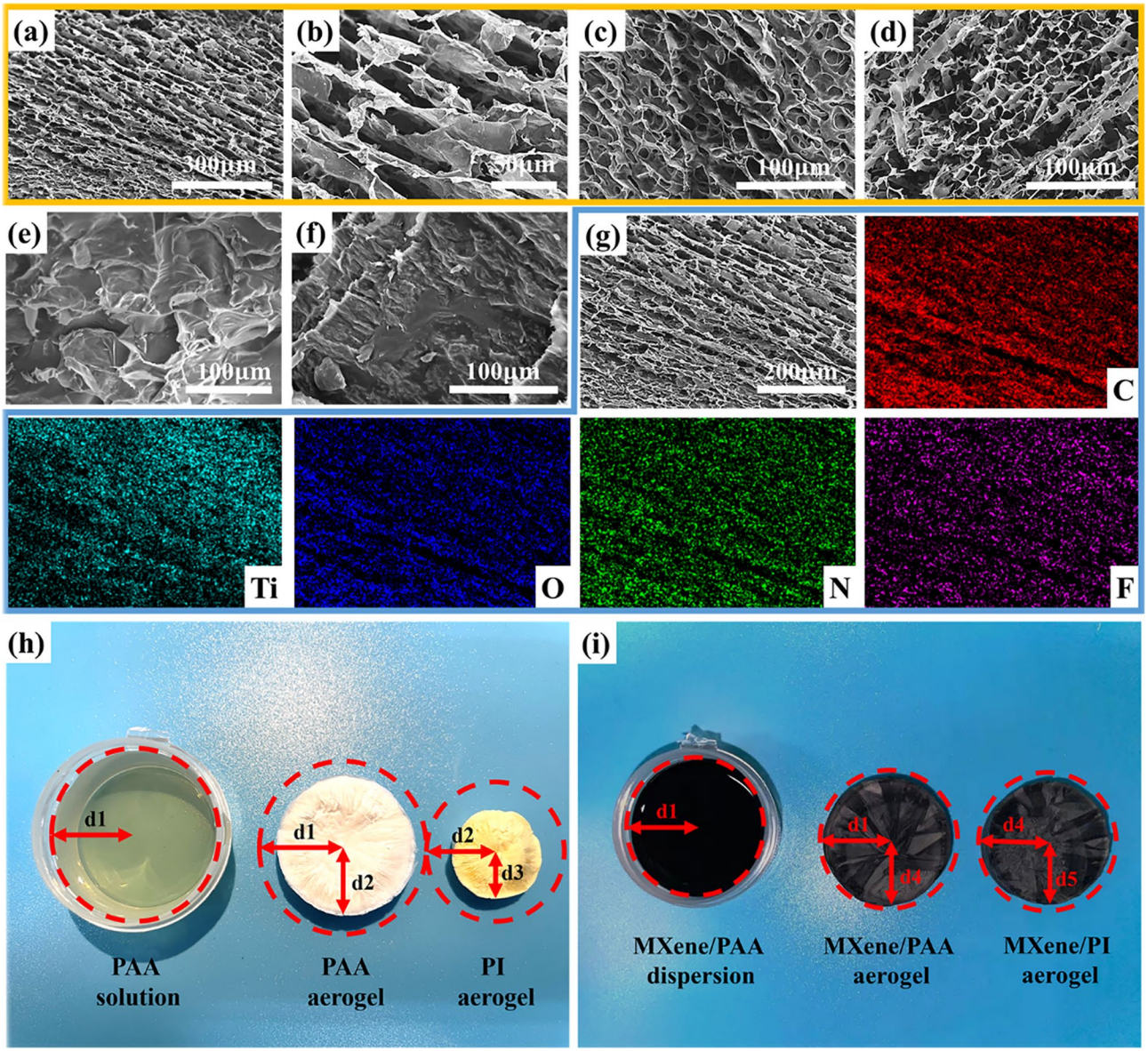

Fig. 3 SEM images of **a**, **b** MP-5, **c** PI aerogel, and **d** MXene aerogel; the cross-section SEM images of **e** PPCC and **f** MPPCC-1; **g** the SEM–EDS characterization of MP-5; aerogel digital photos of **h** PI aerogel and **i** MP-4

and interconnected by PI chains, forming an integrated structure with outstanding size stability.

The EDS mapping image (Fig. 3g) of the MP-5 clearly shows the uniform distribution of MXene nanosheets on the PI backbone, which may completely enhance solar-thermal absorption as well as improve thermal storage ability. The SEM images of PI@PEG phase change composite (PPCC) and MPPCC-1 are shown in Fig. 3e, f. The loose porous structure of PI aerogel and MP-1 have strong capillary driving forces [36], and the interlayer spaces are easily filled by the molten PEG segments. Hence, the interlayer space is porous structure of PI aerogel and MP-1 that are filled with PEG without any gap after vacuum impregnation.

The interactions between the various components in aerogels and MPPCCs were investigated by FTIR (Fig. 4a). The FTIR spectrum of the MXene aerogel shows peaks at 3436.98 cm^{-1} and 1072.36 cm^{-1}, which are –OH and C–O stretching vibrations [45]. The characteristic peaks of MP aerogel appear at 1718.26 cm^{-1} (C = O), 1501.95 cm^{-1} (C = C), 1378.85 cm^{-1} (C–N), and 1243.86 cm^{-1} (C–O) [46], indicating the existing of MXene nanosheets and PI chains. For pure PEG, its characteristic absorption peaks at 3467.38 cm^{-1} and 1108.87 cm^{-1} attribute to the stretching vibrations of –OH and C–O [47]. In addition, the spectra of PPCC and MPPCC-3 show the same characteristic peaks as PEG, and no obvious new peaks are found. These results show that there is physical adsorption between MP and PEG, including capillary effect and hydrogen bond interaction [34]. Therefore, MP can enhance the shape stability of PEG.

The crystal structure of aerogels and MPPCCs were understood using XRD, as shown in Fig. 4b. Compared with the pattern of MXene, the (002) peak intensity of MP is weaker, and the angle of 2θ changes from 6.06 to 5.66°. According to the Bragg equation, the interlayer distance increases from 14.6 to 15.6 Å. This is due to the PI molecules inserting and increasing the interlayer space of MXene nanosheets [48, 49].The curve of pure PEG shows two distinct strong peaks at 19.30° and 23.40°, corresponding to the (120) and (032) planes [6]. Notably, the characteristic peaks of PPCC and MPPCC-3 are similar to those of PEG. These results indicate that there is no change in the crystal structure of PEG in MPPCCs, confirming the porous structure of MP has no effect on the crystallinity of PEG. Therefore, the phase change properties of MPPCCs may not be influenced by the composites structure and keep same as that of pure PEG.

3.3 Phase change properties and thermal reliability of MPPCCs

The phase transition behaviors, including phase transition enthalpy and phase transition temperature, are recorded by DSC measurement. Figure 5a performs the DSC curves of pure PEG and MPPCCs between 20 and 80 °C, and the corresponding parameters are shown in Table 1. In addition, the enthalpy efficiency λ, and the relative enthalpy efficiency η are calculated by formula (1) and (2), respectively. With the little loss of latent heat, the larger values of them are, the more excellent thermal energy storage performance is.

$$\lambda = \frac{\Delta H_{m-MPPCCs}}{\Delta H_{m-PEG}} \times 100\% \quad (1)$$

$$\eta = \frac{\Delta H_{m-MPPCCs}}{\Delta H_{m-PEG} \times \omega} \times 100\% \quad (2)$$

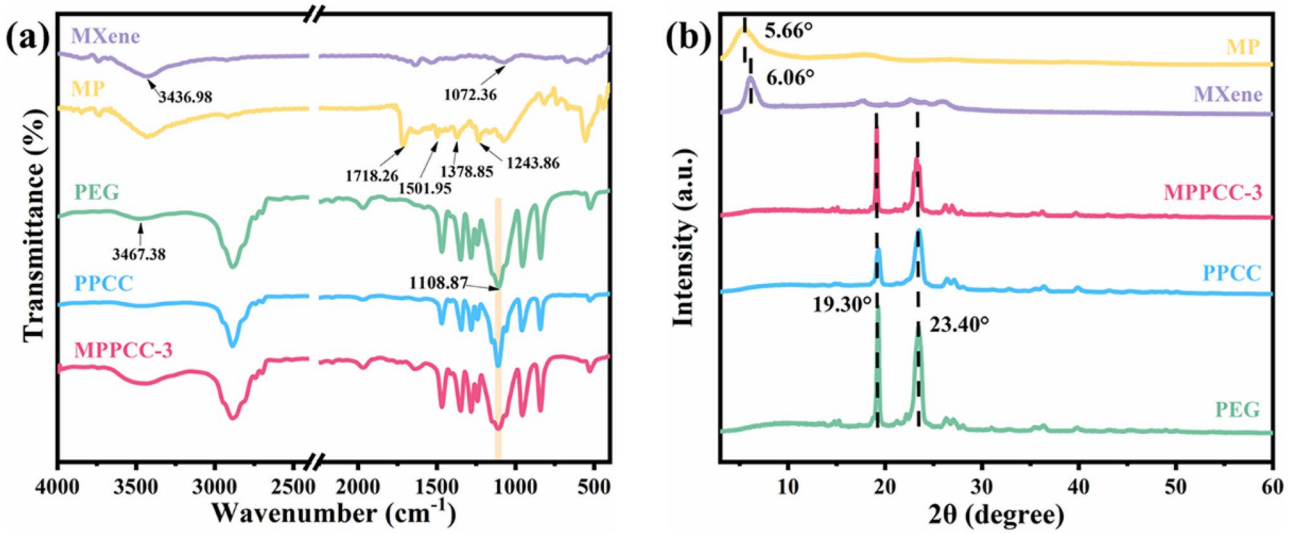

Fig. 4 **a** FTIR spectra and **b** XRD patterns of MXene aerogel, MP, PEG, PPCC, and MPPCC-3

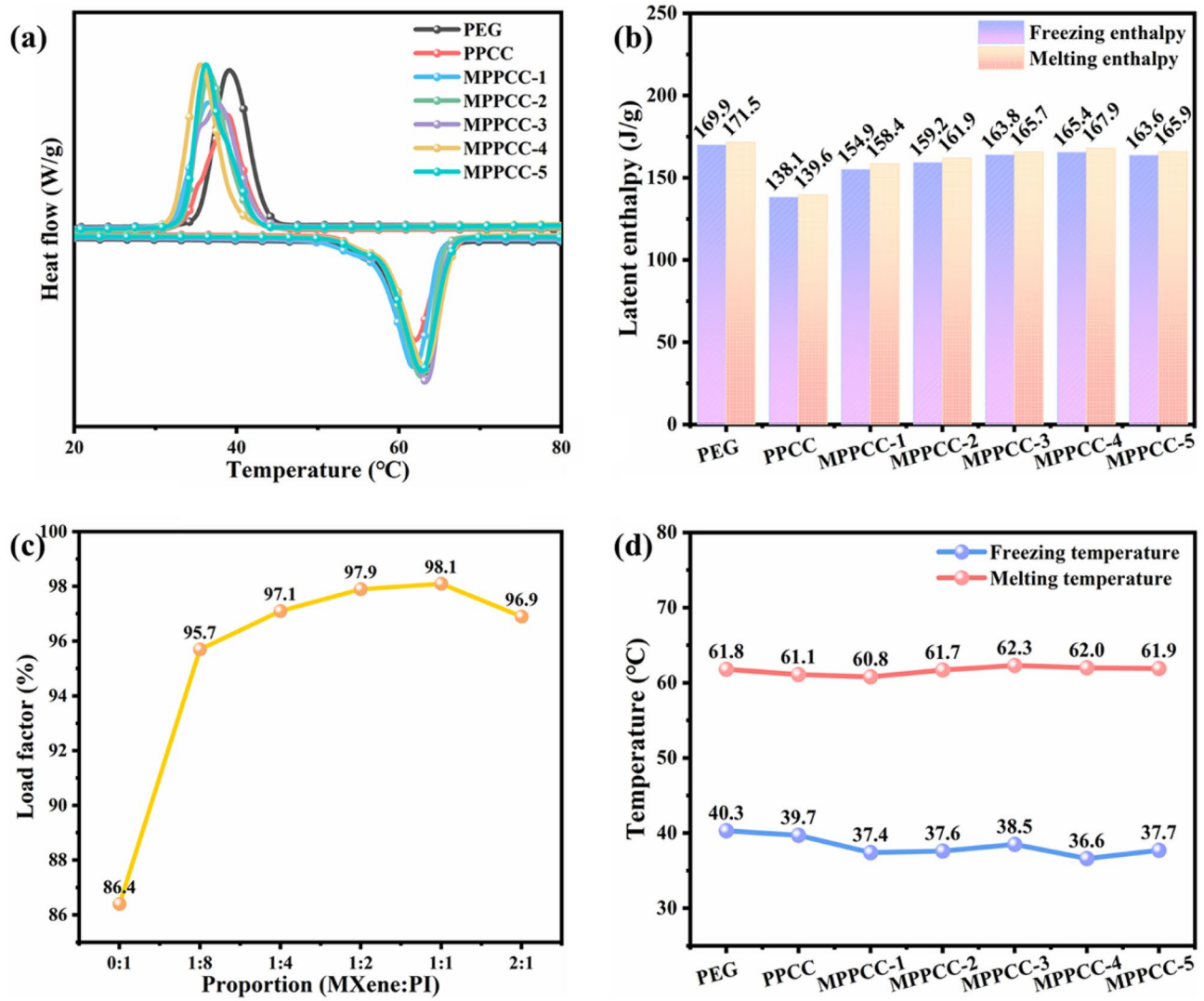

Fig. 5 **a** DSC curves, **b** enthalpy values, **c** loading rate, and **d** peak temperature of PEG and MPPCCs

where $\Delta H_{m-MPPCCs}$ and ΔH_{m-PEG} are the melting enthalpies of MPPCCs and pure PEG, respectively; the ω indicates the loading rate of PEG in MPPCCs.

From Fig. 5b, d and Table 1, it is clear that pure PEG is a good thermal storage material due to its high enthalpy ($\Delta H_m = 171.5$ J/g, $\Delta H_f = 169.9$ J/g) and suitable phase transition temperature ($T_f = 40.3$ °C, $T_m = 61.8$ °C). Compared to pure PEG, the addition of PI aerogel and MPs resulted in significant changes in the melting and freezing peak temperatures of the MPPCCs, as well as in the enthalpy values of melting 139.6 ~ 167.9 J/g and freezing (138.1 ~ 165.4 J/g). These results indicate that MXene

Table 1 Thermal parameters of pure PEG and corresponding MPPCCs

Samples	T_f (°C)	ΔH_f (J/g)	T_m (°C)	ΔH_m (J/g)	λ (%)	ω (%)	η (%)
Pure PEG	40.3	169.9	61.8	171.5	-	-	-
PPCC	39.7	138.1	61.1	139.6	81.3	86.4	94.1
MPPCC-1	37.4	154.9	60.8	158.4	92.4	95.7	96.6
MPPCC-2	37.6	159.2	61.7	161.9	94.4	97.1	97.2
MPPCC-3	38.5	163.8	62.3	165.7	96.6	97.9	98.7
MPPCC-4	36.6	165.4	62.0	167.9	97.9	98.1	99.8
MPPCC-5	37.7	163.6	61.9	165.9	96.7	96.9	99.8

Table 2 Thermal energy storage characteristics of PEG-based phase change composites in literature and the present study

Materials	ΔH_m (J/g)	η (%)	Ref
PEG/epoxy	112.0	68.5	[52]
PEG/wood flour	137.0	73.8	[50]
PEG/potatoes	159.7	77.6	[53]
PEG/MXene	131.2	80.3	[34]
PEG/polyurethane/wood powder	140.2	83.1	[51]
PEG/CaO/$MgCO_3$	193.2	87.3	[54]
PEG/MXene/pomelo peel foam	158.1	95.0	[7]
PEG/carbon nanotube/diatomite	107.4	97.6	[55]
PEG/MXene/PI	167.9	99.8	This work

nanosheets and PI molecules restrict the arrangement and free movement of PEG segments [34]. With the increasing MXene content in MPPCCs, the values of melting and freezing enthalpies firstly increase to a certain value, and then decrease. This shows that the more MXene introduced, the stronger the capillary effect and hydrogen bonding between MPs and PEG, which are conducive to the adsorption of PEG in large quantities. However, the dense pores of aerogels may be performed by excess addition of MXene, leading to decreasing of PEG absorption. As shown in Table 2, MPPCCs still have high relative enthalpy efficiencies compared with related phase change composites [7, 34, 50–55]. Therefore, DSC results show that the construction of MXene/PI framework can well encapsulate PEG to obtain MPPCCs with good thermal storage properties.

Table 3 Thermal parameters of MPPCC-4 thermally cycled 200 times

Samples	T_f (°C)	ΔH_f (J/g)	T_m (°C)	ΔH_m (J/g)	λ (%)
Before	36.6	165.4	62.0	167.9	97.9
Cycle200	36.4	164.3	60.9	165.9	96.7

Excellent thermal reliability and repeatability are the important properties to ensure the long-term utilization in practical solar energy storage applications. The DSC curves of MPPCC-4 before and after 200 thermal cycles are shown in Fig. 6, and the corresponding thermal parameters are recorded in Table 3. There is no significant difference in the DSC curves after 200 thermal cycles, while the value of λ only decreases about 1.2%. This shows that MPPCC-4 has almost no loss of phase change enthalpy after 200 thermal cycles with good thermal reliability and reusability, which can meet the requirements of PCCs in practical solar energy storage applications. Figure 6d, e shows no difference in the position and shape of the peaks of MPPCC-4 before and after 200 thermal cycles as measured by FTIR and XRD spectra, indicating good chemical stability of the MPPCCs to meet practical application requirements.

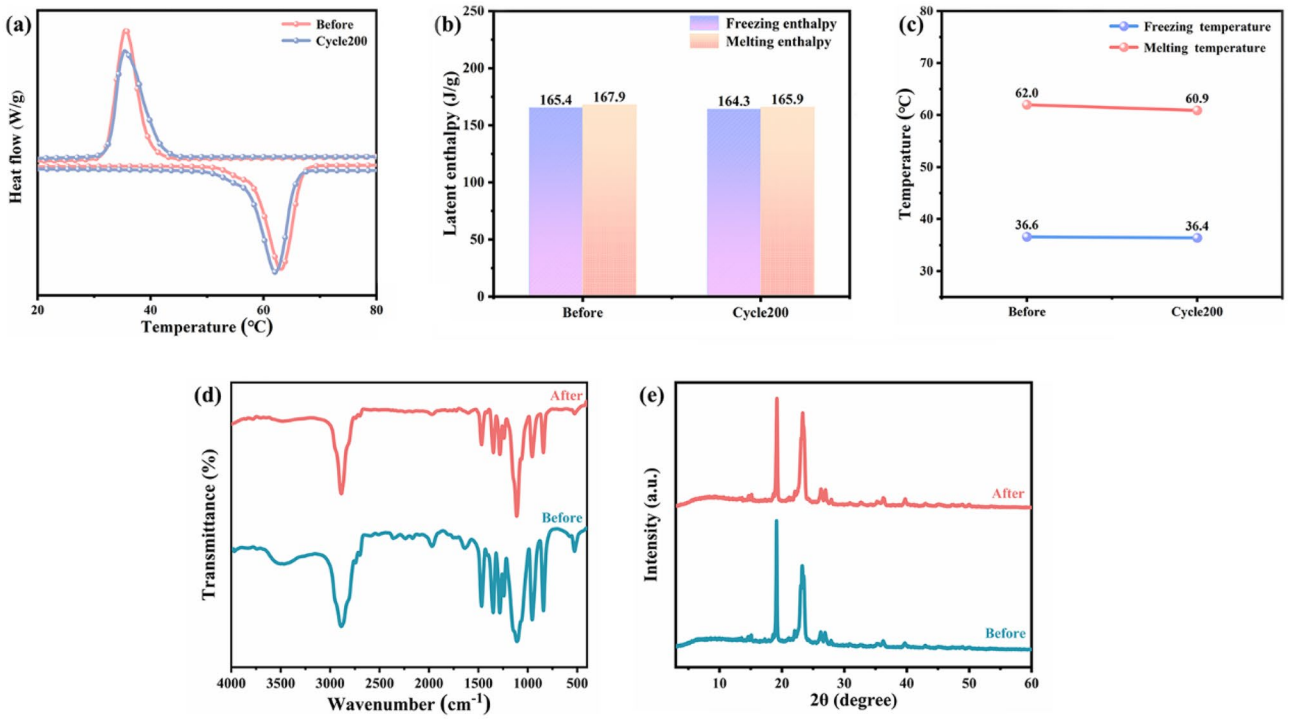

Fig. 6 **a** DSC curves, **b** enthalpy values, **c** peak temperature, **d** FTIR spectra, and **e** XRD patterns of MPPCC-4 thermally cycled 200 times

The shape stability of phase change composites is another key factor for their practical application. As shown in Fig. 7, all samples are placed in a constant temperature vacuum oven at 80 °C. Obviously, pure PEG begins to leak after 30 min heating. However, all MPPCCs maintain their intact shape without any leakage. After 75 min, pure PEG is completely amorphous melting. In contrast, MPPCCs maintain their original shape macroscopically without leakage, suggesting the rigid 3D supporting framework and strong capillary force of MPs are beneficial for PEG absorption. Also, PEG can be tightly fixed via the intermolecular hydrogen bonding interaction between PEG and MPs [36, 56]. All above results confirm that aerogels constructed by PI and MXene show excellent ability to load PEG, and MPPCCs have good shape stability and reliability.

3.4 UV–vis–NIR measurement and solar-thermal conversion of MPPCCs

Figure 8a shows the UV–vis-NIR absorption intensity spectra of pure PEG and MPPCCs. Pure PEG has extremely low absorption over the entire UV–vis-NIR range, even almost zero below 1150 nm. Likewise, the absorbance of PPCC is poor tested. With the introduction of MXene nanosheets, MPPCC-4 and MPPCC-5 exhibit stronger absorbance over the entire spectral range. Furthermore, the absorption intensity of MPPCC-5 is slightly higher than that of MPPCC-4, which can be attributed to relatively higher MXene content of MPPCC-5. Theoretically, stronger light absorption means higher solar-thermal conversion capability, which is beneficial for solar energy storage.

As shown in Fig. 8b, the temperature–time curve (Fig. 8c) and digital thermal infrared imagery (Fig. 8d) of samples were recorded using a homemade infrared thermal imaging data recording device. When the light turns on, the temperature of all samples increased rapidly. When the detected temperature reaches 55 °C, the PEG in the phase change composite undergoes a "solid–liquid" phase transition, the heating rates of all samples start to slow down, and the radiant heat energy is stored in the form of latent heat. After 1390 s, the temperature of PPCC raises to 67.3 °C, while that of MPPCC-4 and MPPCC-5 raise to 78.1 °C and 80.9 °C, respectively. This indicates that the higher the content of MXene nanosheets in MPPCCs, the faster the heating rate and the higher the peak temperature, which is consistent with the UV–vis-NIR results.

When the illumination is stopped at 1390 s, the temperatures of MPPCCs all samples begin to drop rapidly to about 45 °C due to thermal diffusion between the samples and the surrounding environment, and begin to undergo a "liquid–solid" phase transition. The phase transition platform duration of MPPCC-5 during cooling is about 550 s, which is higher than that of MPPCC-4 (530 s) and PPCC (510 s). Due to the higher content of MXene nanosheets,

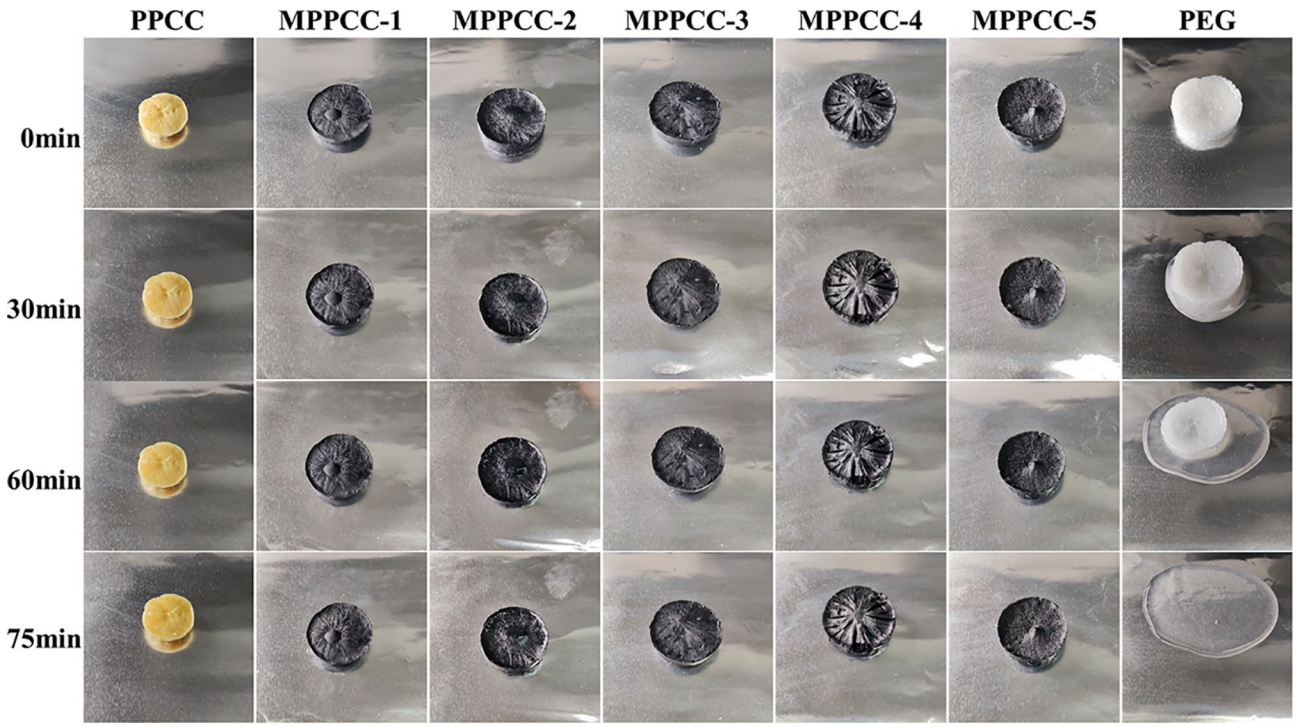

Fig. 7 Macroscopic morphology of pure PEG and MPPCCs at 80 °C

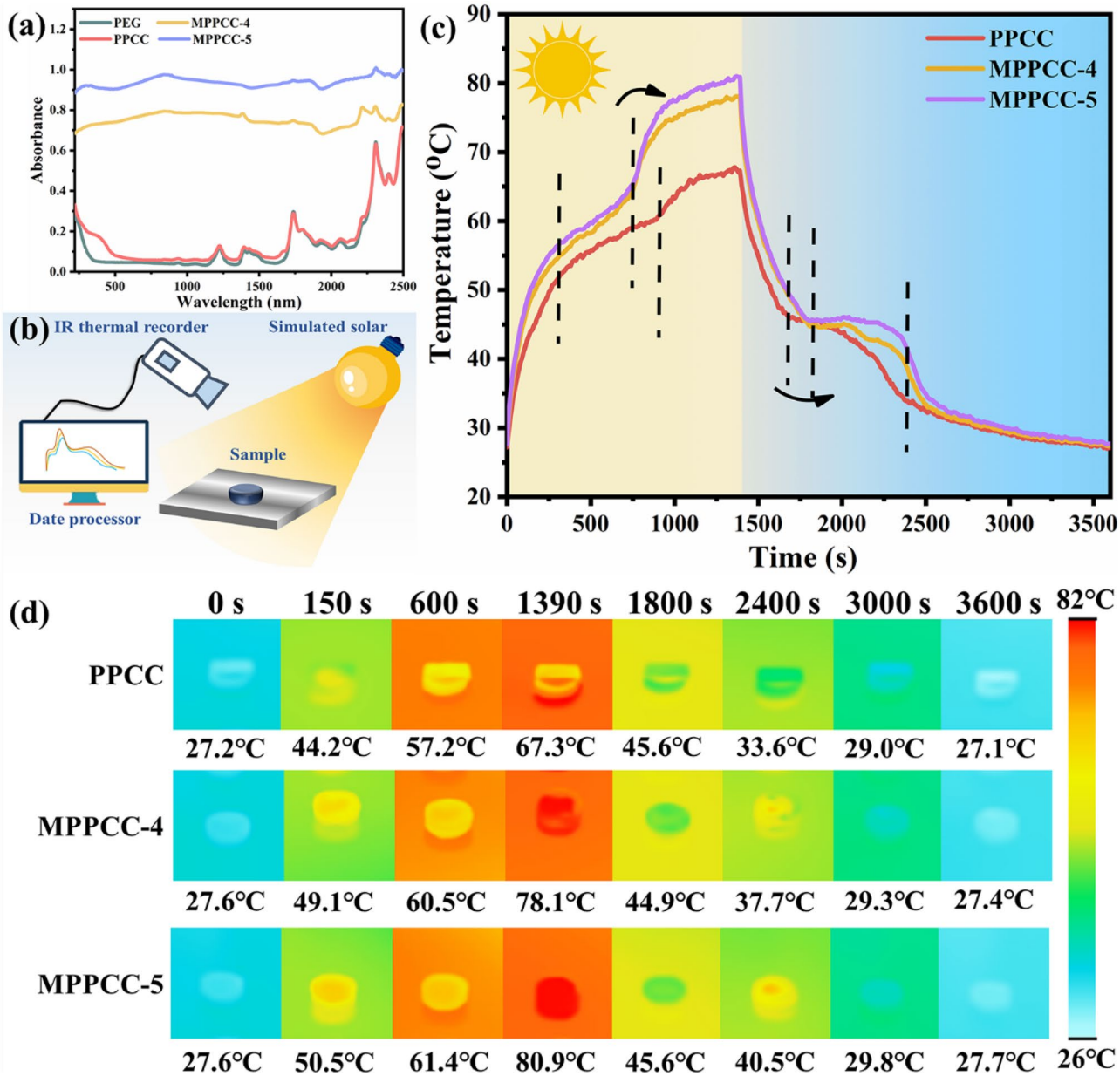

Fig. 8 **a** UV–vis–NIR spectra of PEG and MPPCCs; **b** schematic of the setup for the solar-thermal conversion test; **c** temperature–time curves for MPPCCs during the solar-thermal conversion process; **d** representative thermal infrared images about the solar-thermal conversion performance of MPPCCs with different MXene content

more solar-thermal energy converts into heating latent stored in MPPCC-5 during the same illumination time. Therefore, the heat storage capacity of MPPCC-5 is better than that of MPPCC-4 and PPCC under the same light intensity and duration. Although the PEG loading rate of MPPCC-5 is 1.2% lower than MPPCC-4, there is little effect on the duration of the phase change platform. Meantime, the results of phase change platform duration are consistent with DSC. The above results indicate that the addition of MXene nanosheets is beneficial to improving the solar-thermal conversion ability of MPPCCs. Among them, MPPCC-5 exhibits outstanding solar-thermal conversion ability, following the same trend as the UV–vis-NIR absorption spectrum (Fig. 8a).

Furthermore, the durability of MPPCC-5 under higher light intensity was investigated by solar-thermal conversion cycling experiments (Fig. 9). As shown in Fig. 9a, c, comparing with the phase change platform duration keeping

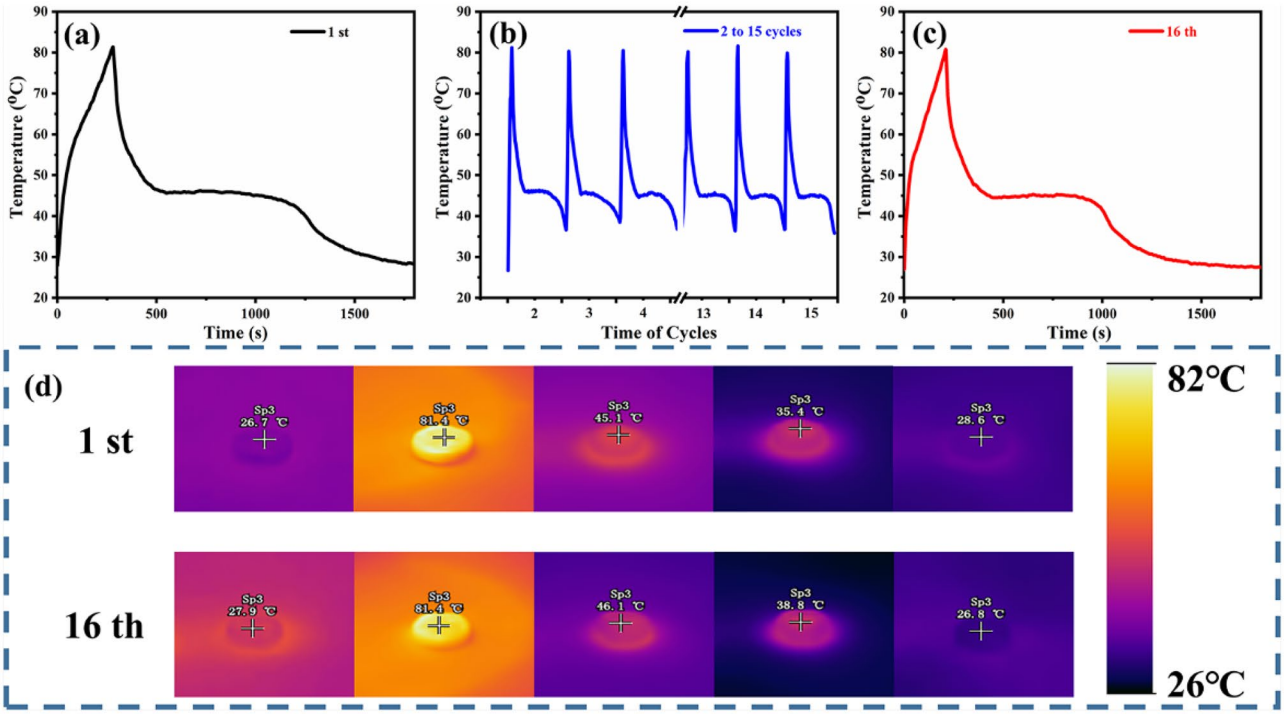

Fig. 9 **a**, **b** and **c** 16 times solar-thermal cycling experiments of MPPCC-5, and **d** the infrared thermal imaging pictures of MPPCC-5 during test of the first and the sixteenth

690 s at the first cycle, the 16th duration of MPPCC-5 is slight shorten to 620 s. However, in Fig. 9b, d, the morphology of MPPCC-5 remains almost unchanged before and after 16 cycles. These results show that MPPCC-5 has excellent solar thermal cycling stability, which provides favorable conditions for long-term thermal storage of phase change composites.

3.5 Thermal stability of MPPCCs

The thermal stability of MXene, PI, MP-4, PEG, and MPPCCs was evaluated by thermogravimetric analysis (TGA). Figure 10 and Table 4 show the corresponding TGA and DTG results. It can be clearly observed from TGA and DTG curves that the thermal decomposition of all samples exhibits one step of mass loss. PEG undergoes a one-stage thermal degradation process corresponding to the pyrolysis of PEG molecular chains, showing a low onset thermal decomposition temperature ($T_{5\%}$, 378.8 °C) and a residual char (2.1%). MXene demonstrates high thermal stability with a mass loss of 12.1%. Furthermore, the PI also possesses high thermal stability, with a high maximum mass loss temperature (T_{max}) of 568.4 °C and residual char of 51.6% at 800 °C. Specifically, in the case of MP-4 exhibits a T_{max} of 587.2 °C and a residual char of 79.9% at 800 °C, indicating the thermal stability of PI can be improved by the addition of MXene. Therefore, the introduction of MXene can effectively hinder the decomposition of the PI matrix by the catalytic charring and barrier effect, thus resulting in improved thermal stability [36, 57].

PEG and all MPPCCs show similar thermal decomposition behavior. It is worth noting that the T_{max} of the MPPCCs is slightly increased with the MXene content increases, which indicates that the thermal degradation of PEG can be inhibited by the MXene. Figure 10f shows the relationship between their final carbon residue as PPCC = 11.5% > MPPCC-1 = 7.5% > MPPCC-5 = 4.3% > MPPCC-4 = 3.3% > PEG = 2.1%. This corresponds to the trend of PEG content contained in the aerogels (Fig. 5c). With the increase of PEG loading rate in MPPCCs, the carbon residue rate decreased. However, compared with PEG, the char residue of MPPCCs was significantly increased, which is attributed to the MXene and PI can change the path of thermal degradation and promote PEG to form carbon residue [36]. The results show that the MPPCCs have sufficient thermal stability under the application conditions (61.7 °C).

3.6 Flammability performance of the MPPCCs

The flame-retardant behavior of MPPCCs was investigated using a micro-combustion calorimeter (MCC). Figure 11 shows the heat release rate (HRR) and total heat release

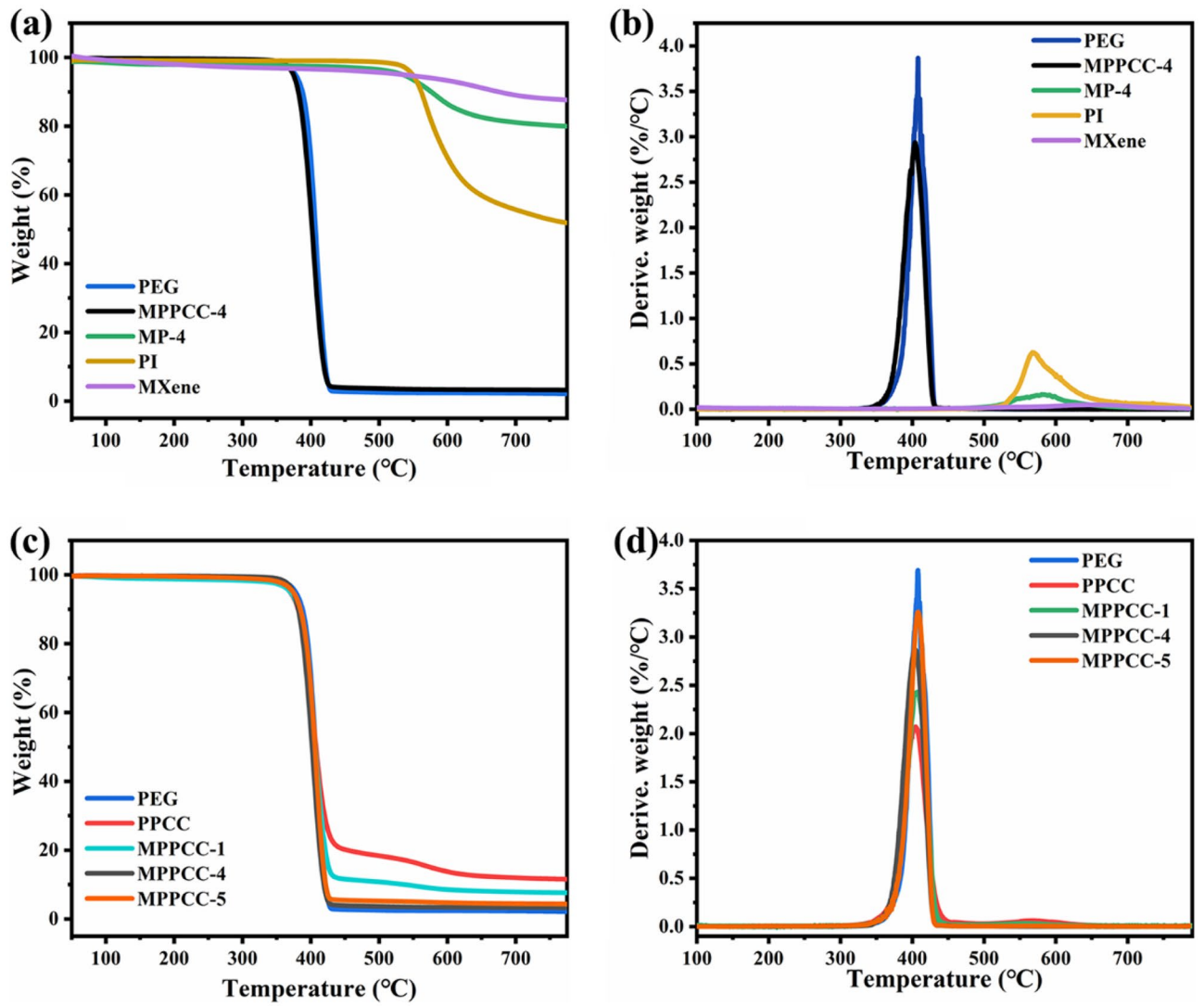

Fig. 10 **a** TGA curves and **b** DTG curves of MXene aerogel, PI aerogel, MP-4, PEG, and MPPCC-4; **c** TGA curves, and **d** DTG curves of PEG and MPPCCs

(THR) curves of PEG, PMPCC-4, and PPCC. The corresponding data, such as peak heat release rate (pHRR), pHRR temperature, and THR, are listed in Table 5. From Fig. 11 and Table 5, it clearly shows that PEG is a flammable material with a high pHRR of 717.2 W/g and a THR of 24.2 kJ/g. By introducing MXene/PI, pHRR and THR of MPPCC-4 are reduced by 26.2% and 11.6%, respectively, compared with those of PEG. The decrease of pHRR and THR in the MXene/PI@PEG system indicates that the introduction of MXene/PI effectively decreases the heat release, thereby enhancing flame retardancy. The phenomenon is mainly due to the presence of MXene, which can contribute to improving the formation of a thermostable char, and the Ti-containing residual char can inhibit the underlying matrix from further burning [38, 58]. The SEM energy spectroscopy (EDS) results of MPPCC-4 before and after combustion (Fig. 12c_1, c_2) also demonstrate the protective effect of Ti-containing char during combustion.

Table 4 TGA results for MXene, PI, MP-4, PEG, and MPPCCs in nitrogen atmosphere

Samples	$T_{5\%}$ (°C)	T_{max} (°C)	Char residues at 800 °C (%)
MXene	536.3	660.8	87.9
PI	552.5	568.4	51.6
MP-4	554.4	587.2	79.9
PEG	378.8	407.7	2.1
PPCC	371.0	401.8	11.5
MPPCC-1	371.3	403.0	7.5
MPPCC-4	375.0	404.8	3.3
MPPCC-5	375.4	408.9	4.3

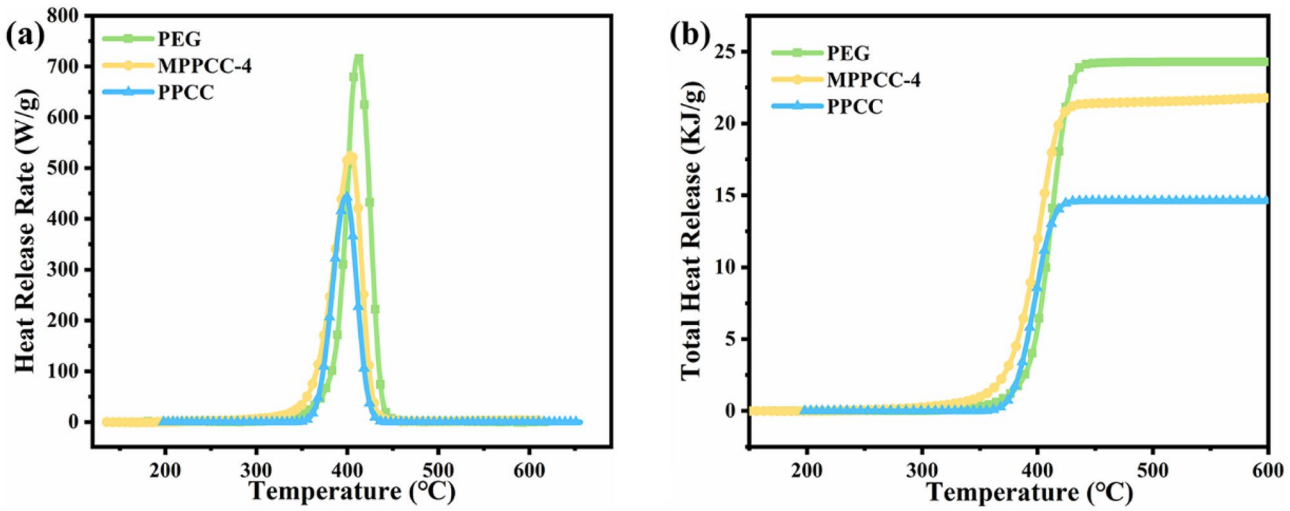

Fig. 11 **a** Heat release rate and **b** total heat release versus temperature curves of the samples

Table 5 MCC data of the samples

Samples	pHRR (W/g)	pHRR (°C)	THR (kJ/g)
PEG	717.2	411.1	24.2
MPPCC-4	529.3	403.7	21.4
PPCC	444.0	398.4	14.6

However, compared with MPPCC-4, the pHRR and THR of PPCC decreased by 16.1% and 31.8%, respectively. The reason is due to a load of PEG in PPCC being 11.7% less than in MPPCC-4 and thus weakening the heat release.

The microstructures of the residues were investigated by SEM. According to Fig. 12a_1, a_2, the PPCC show honeycomb-like structures, which are similar to the skeleton of PI. This indicates that almost all such PEG in PPCC is thermally decomposed and unable to form carbon residue. In contrast, a large number of fragments of char residues can be observed for MPPCC-4 residues, as shown in Fig. 12b_1, b_2. Such phenomenon demonstrates that the MXene can promote charring of the pyrolysis products of PEG by catalytic effect and thus improve the formation of stable graphitized char, which results in reduced heat release and reinforces the flame retardancy.

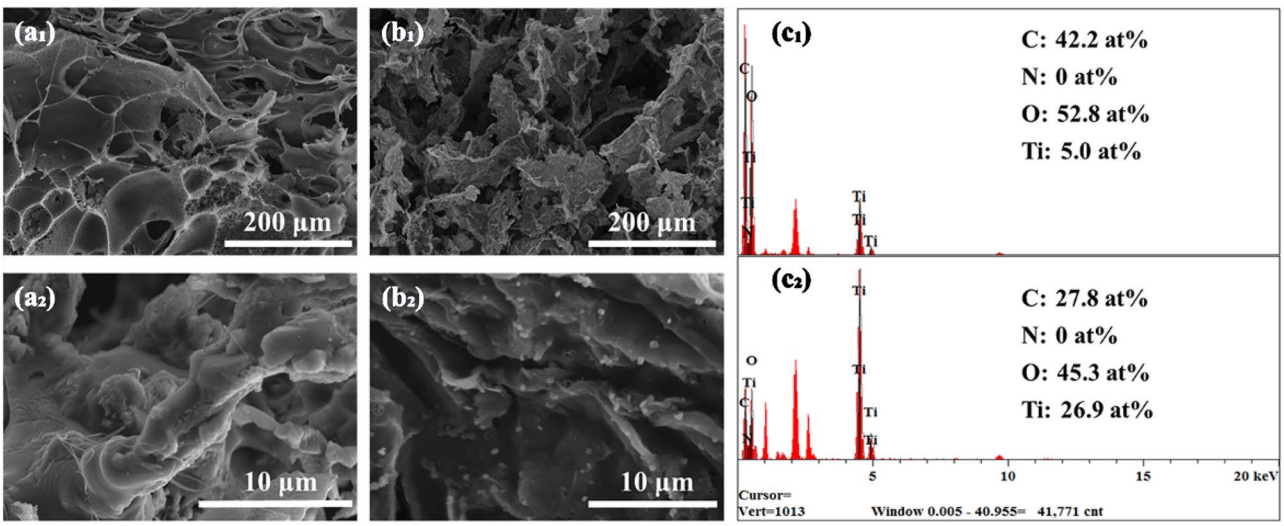

Fig. 12 SEM images of $\mathbf{a_1}$, $\mathbf{a_2}$ burned PPCC and $\mathbf{b_1}$, $\mathbf{b_2}$ burned MPPCC-4; EDS element spectrum and atomic percentage of $\mathbf{c_1}$ MPPCC-4 and $\mathbf{c_2}$ burned MPPCC-4

4 Conclusions

In this work, 2D layered MXene nanosheets with excellent photothermal effect were synthesized via in-situ HF method. Afterwards, MPs were freeze-dried and thermally annealed before being impregnated with PEG to create leakage-proof MPPCCs. MPPCC-4 has high PEG loading capacity (98.1%) and thermal storage density (167.9 J/g), performing excellent solar thermal conversion capacity. In addition, the coordinated effect of MXene nanosheets and PI significantly reduced the HRR and THR of MPPCCs, while the carbon yield increased, indicating that the flame retardancy of MPPCCs was significantly improved. In conclusion, MPPCCs have extremely high thermal storage density, excellent flame retardancy, and good solar-thermal conversion ability, showing a considerable potential in the field of solar energy utilization.

Supplementary Information The online version contains supplementary material available at https://doi.org/10.1007/s42114-022-00504-4.

Funding This work was supported by the National Natural Science Foundation of China (Grant Nos. U20A20299 and 52003111). X. S. received support from the Research Fund Program of Yunnan Provincial Key Laboratory of Energy Saving in Phosphorus Chemical Engineering and New Phosphorus Materials (Grant No. LHG-2020–0004). Y. C. was supported by the Guangdong Special Support Program (Grant No. 2017TX04N371). J. H. received support from the Opening Project of Key Laboratory of Polymer Processing Engineering (South China University of Technology), Ministry of Education, (Grant No. KFKT2001). The authors also received financial support from Taif University Researchers Supporting Project number (TURSP-2020/158), Taif University, Taif, Saudi Arabia.

Declarations

Conflict of interest The authors declare no competing interests.

References

1. Nazir H, Batool M, Bolivar Osorio FJ et al (2019) Recent developments in phase change materials for energy storage applications: a review. Int J Heat Mass Transf 129:491–523. https://doi.org/10.1016/j.ijheatmasstransfer.2018.09.126
2. Xie Y, Li W, Huang H et al (2020) Bio-based Radish@PDA/PEG sandwich composite with high efficiency solar thermal energy storage. ACS Sustainable Chem Eng 8:8448–8457. https://doi.org/10.1021/acssuschemeng.0c02959
3. Huang J, Lyu S, Han H et al (2022) Enhanced looping biomass/vapour gasification utilizing waste heat from molten copper slags. Energy. https://doi.org/10.1016/j.energy.2022.123962
4. Pandey AK, Hossain MS, Tyagi VV et al (2018) Novel approaches and recent developments on potential applications of phase change materials in solar energy. Renew Sustain Energy Rev 82:281–323. https://doi.org/10.1016/j.rser.2017.09.043
5. Lin Y, Jia Y, Alva G, Fang G (2018) Review on thermal conductivity enhancement, thermal properties and applications of phase change materials in thermal energy storage. Renew Sustain Energy Rev 82:2730–2742. https://doi.org/10.1016/j.rser.2017.10.002
6. Du Y, Huang H, Hu X et al (2021) Melamine foam/polyethylene glycol composite phase change material synergistically modified by polydopamine/MXene with enhanced solar-to-thermal conversion. Renewable Energy 171:1–10. https://doi.org/10.1016/j.renene.2021.02.077
7. Sheng X, Dong D, Lu X et al (2020) MXene-wrapped bio-based pomelo peel foam/polyethylene glycol composite phase change material with enhanced light-to-thermal conversion efficiency, thermal energy storage capability and thermal conductivity. Compos A Appl Sci Manuf 138:106067. https://doi.org/10.1016/j.compositesa.2020.106067
8. Huang X, Chen X, Li A et al (2019) Shape-stabilized phase change materials based on porous supports for thermal energy storage applications. Chem Eng J 356:641–661. https://doi.org/10.1016/j.cej.2018.09.013
9. Chen R, Yao R, Xia W, Zou R (2015) Electro/photo to heat conversion system based on polyurethane embedded graphite foam. Appl Energy 152:183–188. https://doi.org/10.1016/j.apenergy.2015.01.022
10. Sun Z, Shi T, Wang Y et al (2022) Hierarchical microencapsulation of phase change material with carbon-nanotubes/polydopamine/silica shell for synergistic enhancement of solar photothermal conversion and storage. Sol Energy Mater Sol Cells 236:111539. https://doi.org/10.1016/j.solmat.2021.111539
11. Li X, Sheng M, Gong S et al (2022) Flexible and multifunctional phase change composites featuring high-efficiency electromagnetic interference shielding and thermal management for use in electronic devices. Chem Eng J 430:132928. https://doi.org/10.1016/j.cej.2021.132928
12. Zhou Y, Wang X, Liu X et al (2019) Polyurethane-based solid-solid phase change materials with halloysite nanotubes-hybrid graphene aerogels for efficient light- and electro-thermal conversion and storage. Carbon 142:558–566. https://doi.org/10.1016/j.carbon.2018.10.083
13. Li G, Zhang X, Wang J, Fang J (2016) From anisotropic graphene aerogels to electron- and photo-driven phase change composites. J Mater Chem A 4:17042–17049. https://doi.org/10.1039/C6TA07587H
14. Wang L, Shi X, Zhang J et al (2020) Lightweight and robust rGO/sugarcane derived hybrid carbon foams with outstanding EMI shielding performance. J Mater Sci Technol 52:119–126. https://doi.org/10.1016/j.jmst.2020.03.029
15. Zhao Y, Liu F, Zhu K et al (2022) Three-dimensional printing of the copper sulfate hybrid composites for supercapacitor electrodes with ultra-high areal and volumetric capacitances. Adv Compos Hybrid Mater. https://doi.org/10.1007/s42114-022-00430-5
16. Lu B, Zhang Y, Sun D, Jing X (2021) Experimental investigation on thermal properties of paraffin/expanded graphite composite material for low temperature thermal energy storage. Renewable Energy 178:669–678. https://doi.org/10.1016/j.renene.2021.06.070
17. Wu M, Li T, Wang P et al (2021) Dual-encapsulated highly conductive and liquid-free phase change composites enabled by polyurethane/graphite nanoplatelets hybrid networks for efficient energy storage and thermal management. Small. https://doi.org/10.1002/smll.202105647
18. Hu X, Wu H, Lu X et al (2021) Improving thermal conductivity of ethylene propylene diene monomer/paraffin/expanded graphite shape-stabilized phase change materials with great thermal management potential via green steam explosion. Adv Compos Hybrid Mater 4:478–491. https://doi.org/10.1007/s42114-021-00300-6
19. Han Y, Ruan K, Gu J (2022) Janus (BNNS/ANF)-(AgNWs/ANF) thermal conductivity composite films with superior electromagnetic interference shielding and Joule heating performances. Nano Res 15:4747–4755. https://doi.org/10.1007/s12274-022-4159-z
20. Gong S, Li X, Sheng M et al (2021) High thermal conductivity and mechanical strength phase change composite with double supporting skeletons for industrial waste heat recovery. ACS Appl

Mater Interfaces 13:47174–47184. https://doi.org/10.1021/acsami.1c15670
21. Dong J, Cao L, Li Y et al (2020) Largely improved thermal conductivity of PI/BNNS nanocomposites obtained by constructing a 3D BNNS network and filling it with AgNW as the thermally conductive bridges. Compos Sci Technol 196:108242. https://doi.org/10.1016/j.compscitech.2020.108242
22. Pan D, Yang G, Abo-Dief HM et al (2022) Vertically aligned silicon carbide nanowires/boron nitride cellulose aerogel networks enhanced thermal conductivity and electromagnetic absorbing of epoxy composites. Nano-Micro Lett 14:118. https://doi.org/10.1007/s40820-022-00863-z
23. Yang L, Yang J, Tang L-S et al (2020) Hierarchically porous PVA aerogel for leakage-proof phase change materials with superior energy storage capacity. Energy Fuels 34:2471–2479. https://doi.org/10.1021/acs.energyfuels.9b04212
24. Xu H, Yin X, Li X et al (2019) Lightweight Ti_2CT_x MXene/poly(vinyl alcohol) composite foams for electromagnetic wave shielding with absorption-dominated feature. ACS Appl Mater Interfaces 11:10198–10207. https://doi.org/10.1021/acsami.8b21671
25. Zhang Y, Yan Y, Qiu H et al (2022) A mini-review of MXene porous films: preparation, mechanism and application. J Mater Sci Technol 103:42–49. https://doi.org/10.1016/j.jmst.2021.08.001
26. Zhang Y, Ma Z, Ruan K, Gu J (2022) Multifunctional $Ti_3C_2T_x$-(Fe_3O_4/polyimide) composite films with Janus structure for outstanding electromagnetic interference shielding and superior visual thermal management. Nano Res 15:5601–5609. https://doi.org/10.1007/s12274-022-4358-7
27. Song P, Liu B, Qiu H et al (2021) MXenes for polymer matrix electromagnetic interference shielding composites: a review. Compos Commun 24:100653. https://doi.org/10.1016/j.coco.2021.100653
28. Dong Y, Chertopalov S, Maleski K et al (2018) Saturable absorption in 2D Ti_3C_2 MXene thin films for passive photonic diodes. Adv Mater 30:1705714. https://doi.org/10.1002/adma.201705714
29. Gong S, Sheng X, Li X et al (2022) A multifunctional flexible composite film with excellent multi-source driven thermal management, electromagnetic interference shielding, and fire safety performance, inspired by a "brick–mortar" sandwich structure. Adv Funct Materials. https://doi.org/10.1002/adfm.202200570
30. Xing C, Chen S, Liang X et al (2018) Two-dimensional MXene (Ti_3C_2)-integrated cellulose hydrogels: toward smart three-dimensional network nanoplatforms exhibiting light-induced swelling and bimodal photothermal/chemotherapy anticancer activity. ACS Appl Mater Interfaces 10:27631–27643. https://doi.org/10.1021/acsami.8b08314
31. Fan X, Liu L, Jin X et al (2019) MXene $Ti_3C_2T_x$ for phase change composite with superior photothermal storage capability. J Mater Chem A 7:14319–14327. https://doi.org/10.1039/C9TA03962G
32. Du X, Qiu J, Deng S et al (2020) $Ti_3C_2T_x$@PDA-integrated polyurethane phase change composites with superior solar-thermal conversion efficiency and improved thermal conductivity. ACS Sustainable Chem Eng 8:5799–5806. https://doi.org/10.1021/acssuschemeng.0c01582
33. Xu D, Li Z, Li L, Wang J (2020) Insights into the photothermal conversion of 2D MXene nanomaterials: synthesis, mechanism, and applications. Adv Func Mater 30:2000712. https://doi.org/10.1002/adfm.202000712
34. Lu X, Huang H, Zhang X et al (2019) Novel light-driven and electro-driven polyethylene glycol/two-dimensional MXene form-stable phase change material with enhanced thermal conductivity and electrical conductivity for thermal energy storage. Compos B Eng 177:107372. https://doi.org/10.1016/j.compositesb.2019.107372
35. Yu B, Yuen ACY, Xu X et al (2021) Engineering MXene surface with POSS for reducing fire hazards of polystyrene with enhanced thermal stability. J Hazard Mater 401:123342. https://doi.org/10.1016/j.jhazmat.2020.123342
36. Luo Y, Xie Y, Jiang H et al (2021) Flame-retardant and form-stable phase change composites based on MXene with high thermostability and thermal conductivity for thermal energy storage. Chem Eng J 420:130466. https://doi.org/10.1016/j.cej.2021.130466
37. Wang L, Ma Z, Zhang Y et al (2022) Mechanically strong and folding-endurance $Ti_3C_2T_x$ MXene/PBO nanofiber films for efficient electromagnetic interference shielding and thermal management. Carbon Energy 4:200–210. https://doi.org/10.1002/cey2.174
38. Huang S, Wang L, Li Y et al (2021) Novel $Ti_3C_2T_x$ MXene/epoxy intumescent fire-retardant coatings for ancient wooden architectures. J Appl Polym Sci 138:50649. https://doi.org/10.1002/app.50649
39. Zhang Z, Wang X, Zu G et al (2019) Resilient, fire-retardant and mechanically strong polyimide-polyvinylpolymethylsiloxane composite aerogel prepared via stepwise chemical liquid deposition. Mater Des 183:108096. https://doi.org/10.1016/j.matdes.2019.108096
40. Chen L, Xu Z, Wang F et al (2020) A flame-retardant and transparent wood/polyimide composite with excellent mechanical strength. Compos Commun 20:100355. https://doi.org/10.1016/j.coco.2020.05.001
41. Lin P, Xie J, He Y et al (2020) MXene aerogel-based phase change materials toward solar energy conversion. Sol Energy Mater Sol Cells 206:110229. https://doi.org/10.1016/j.solmat.2019.110229
42. Rasool K, Mahmoud KA, Johnson DJ et al (2017) Efficient antibacterial membrane based on two-dimensional $Ti_3C_2T_x$ (MXene) nanosheets. Sci Rep 7:1598. https://doi.org/10.1038/s41598-017-01714-3
43. Shahzad F, Iqbal A, Zaidi SA et al (2019) Nafion-stabilized two-dimensional transition metal carbide ($Ti_3C_2T_x$ MXene) as a high-performance electrochemical sensor for neurotransmitter. J Ind Eng Chem 79:338–344. https://doi.org/10.1016/j.jiec.2019.03.061
44. Wang N-N, Wang H, Wang Y-Y et al (2019) Robust, lightweight, hydrophobic, and fire-retarded polyimide/MXene aerogels for effective oil/water separation. ACS Appl Mater Interfaces 11:40512–40523. https://doi.org/10.1021/acsami.9b14265
45. He X, Li S, Shen R et al (2022) A high-performance waterborne polymeric composite coating with long-term anti-corrosive property based on phosphorylation of chitosan-functionalized $Ti_3C_2T_x$ MXene. Adv Compos Hybrid Mater. https://doi.org/10.1007/s42114-021-00392-0
46. Qin Y, Peng Q, Ding Y et al (2015) Lightweight, superelastic, and mechanically flexible graphene/polyimide nanocomposite foam for strain sensor application. ACS Nano 9:8933–8941. https://doi.org/10.1021/acsnano.5b02781
47. He L, Wang H, Yang F, Zhu H (2018) Preparation and properties of polyethylene glycol/unsaturated polyester resin/graphene nanoplates composites as form-stable phase change materials. Thermochim Acta 665:43–52. https://doi.org/10.1016/j.tca.2018.04.012
48. Liu J, Zhang H-B, Xie X et al (2018) Multifunctional, superelastic, and lightweight MXene/polyimide aerogels. Small 14:1802479. https://doi.org/10.1002/smll.201802479
49. Dai Y, Wu X, Liu Z et al (2020) Highly sensitive, robust and anisotropic MXene aerogels for efficient broadband microwave absorption. Compos B Eng 200:108263. https://doi.org/10.1016/j.compositesb.2020.108263
50. Liang B, Lu X, Li R et al (2019) Solvent-free preparation of bio-based polyethylene glycol/wood flour composites as novel shape-stabilized phase change materials for solar thermal energy storage. Sol Energy Mater Sol Cells 200:110037. https://doi.org/10.1016/j.solmat.2019.110037
51. Lu X, Liang B, Sheng X et al (2020) Enhanced thermal conductivity of polyurethane/wood powder composite phase change

materials via incorporating low loading of graphene oxide nanosheets for solar thermal energy storage. Sol Energy Mater Sol Cells 208:110391. https://doi.org/10.1016/j.solmat.2019.110391
52. Wu B, Jiang Y, Wang Y et al (2018) Study on a PEG/epoxy shape-stabilized phase change material: preparation, thermal properties and thermal storage performance. Int J Heat Mass Transf 126:1134–1142. https://doi.org/10.1016/j.ijheatmasstransfer.2018.05.153
53. Zhao Y, Min X, Huang Z et al (2018) Honeycomb-like structured biological porous carbon encapsulating PEG: a shape-stable phase change material with enhanced thermal conductivity for thermal energy storage. Energy Build 158:1049–1062. https://doi.org/10.1016/j.enbuild.2017.10.078
54. Zahir MdH, Irshad K, Aziz MdA et al (2019) Shape-stabilized phase change material for solar thermal energy storage: CaO containing $MgCO_3$ mixed with polyethylene glycol. Energy Fuels 33:12041–12051. https://doi.org/10.1021/acs.energyfuels.9b02885
55. Qian T, Zhu S, Wang H, Fan B (2019) Comparative study of carbon nanoparticles and single-walled carbon nanotube for light-heat conversion and thermal conductivity enhancement of the multifunctional PEG/diatomite composite phase change material. ACS Appl Mater Interfaces 11:29698–29707. https://doi.org/10.1021/acsami.9b04349
56. Yang J, Qi G-Q, Liu Y et al (2016) Hybrid graphene aerogels/phase change material composites: thermal conductivity, shape-stabilization and light-to-thermal energy storage. Carbon 100:693–702. https://doi.org/10.1016/j.carbon.2016.01.063
57. Huang H, Dong D, Li W et al (2020) Synergistic effect of MXene on the flame retardancy and thermal degradation of intumescent flame retardant biodegradable poly (lactic acid) composites. Chin J Chem Eng 28:1981–1993. https://doi.org/10.1016/j.cjche.2020.04.014
58. Mao M, Yu K-X, Cao C-F et al (2022) Facile and green fabrication of flame-retardant $Ti_3C_2T_x$ MXene networks for ultrafast, reusable and weather-resistant fire warning. Chem Eng J 427:131615. https://doi.org/10.1016/j.cej.2021.131615